PNAS RESEARCH ARTICLE | PLANT BIOLOGY OPEN ACCESS

Tree architecture: A strigolactone-deficient mutant reveals a connection between branching order and auxin gradient along the tree stem

Chang Su[a,b], Andrzej Kokosza[c,1], Xiaonan Xie[d,1], Aleš Pěnčík[e], Youjun Zhang[f,g], Pasi Raumonen[h], Xueping Shi[i], Sampo Muranen[a,b], Melis Kucukoglu Topcu[a,b], Juha Immanen[a,j], Risto Hagqvist[j], Omid Safronov[a,k], Juan Alonso-Serra[l], Gugan Eswaran[a,b], Mirko Pavicic Venegas[m,n], Karin Ljung[o], Sally Ward[p], Ari Pekka Mähönen[a,b], Kristiina Himanen[a,n], Jarkko Salojärvi[a,q], Alisdair R. Fernie[f,g], Ondřej Novák[e,r], Ottoline Leyser[p], Wojtek Pałubicki[c], Ykä Helariutta[a,b,p], and Kaisa Nieminen[a,j,2]

Edited by R. Poethig, University of Pennsylvania, Philadelphia, PA; received May 23, 2023; accepted October 20, 2023

Due to their long lifespan, trees and bushes develop higher order of branches in a perennial manner. In contrast to a tall tree, with a clearly defined main stem and branching order, a bush is shorter and has a less apparent main stem and branching pattern. To address the developmental basis of these two forms, we studied several naturally occurring architectural variants in silver birch (*Betula pendula*). Using a candidate gene approach, we identified a bushy *kanttarelli* variant with a loss-of-function mutation in the *BpMAX1* gene required for strigolactone (SL) biosynthesis. While *kanttarelli* is shorter than the wild type (WT), it has the same number of primary branches, whereas the number of secondary branches is increased, contributing to its bush-like phenotype. To confirm that the identified mutation was responsible for the phenotype, we phenocopied *kanttarelli* in transgenic *BpMAX1::RNAi* birch lines. SL profiling confirmed that both *kanttarelli* and the transgenic lines produced very limited amounts of SL. Interestingly, the auxin (IAA) distribution along the main stem differed between WT and *BpMAX1::RNAi*. In the WT, the auxin concentration formed a gradient, being higher in the uppermost internodes and decreasing toward the basal part of the stem, whereas in the transgenic line, this gradient was not observed. Through modeling, we showed that the different IAA distribution patterns may result from the difference in the number of higher-order branches and plant height. Future studies will determine whether the IAA gradient itself regulates aspects of plant architecture.

tree architecture | branching modeling | strigolactones | auxin distribution | *Betula pendula*

Significance

What makes a tree a tree instead of a bush? Through a candidate gene approach, we identified a natural bush-like (short and highly branching) SL-deficient birch mutant, *kanttarelli*, with an early *STOP* codon in an essential SL biosynthesis gene, *BpMAX1*. The number of higher-order branches was increased in the mutant and in phenocopying transgenic *RNAi* -lines. Intriguingly, the auxin concentration formed a gradient along the main stem in the WT, with more auxin in the uppermost internodes and less toward the base, whereas in the transgenic line this gradient was absent. Mathematical modeling showed that this difference in auxin distribution may result from the differing architectures. Our results could be applied in the breeding of trees with an optimized architecture.

Woody plants display two major forms in nature, growing as either a tree or a bush. A tree is tall, with a clearly defined main stem, while bushes are short without an evident main stem, and they produce an abundance of branches (1). Tree architecture is a three-dimensional concept describing all of the aerial elements of the plant, including its stem shape, branching pattern, leaves, and reproductive organs, all composing a functional general structure. The long lifespan of perennial woody species allows trees and bushes to grow taller and add higher-order branches annually (2–5). Vegetative shoot development occurs in repeating modules called phytomers, each composed of a leaf, an axillary meristem, and an internode (6). Axillary buds produced by axillary meristems can either stay dormant or branch out (Fig. 1*A*). As such, they provide a high degree of phenotypic plasticity for tree growth. The number, size, and angle of branches determine the overall form and architecture of a tree.

The process of architectural development differs fundamentally between tree species. Some species tend to have a relatively long period of unbranched growth characterized by very limited primary branching of the main stem. For instance, under greenhouse conditions, *Populus* spp. generally do not develop primary branches until they are over ca. 1.5 m in length (ca. 3 mo old). In contrast, some tree species already develop primary branches as seedlings; e.g., birch (*Betula* spp.) seedlings generally branch out when they are only ca. 25 cm (less than 1 mo old) under greenhouse conditions, which makes it possible to study complex architectural traits in young birch trees. Furthermore, birches have highly variable naturally occurring architectural forms; they display a wide architectural spectrum from small bushes to tall trees. In *Betula* spp., almost all of the axillary buds on the main stem grow out at a young age. Besides its architectural variance, birch is also attractive to researchers because of the multiple genomic (7) and transcriptomic resources (8) that are available, together with well-established genetic tools (9, 10). We therefore focused our study on the genetic basis of architectural development in trees on silver birch (*Betula pendula*). Through a candidate gene approach of several naturally occurring architectural birch variants, we identified one, *kanttarelli*, having an early *STOP* codon in an essential strigolactone (SL)

The authors declare no competing interest.

This article is a PNAS Direct Submission.

[1]A.K. and X.X. contributed equally to this work.

[2]To whom correspondence may be addressed. Email: kaisa.p.nieminen@luke.fi.

This article contains supporting information online at https://www.pnas.org/lookup/suppl/doi:10.1073/pnas.2308587120/-/DCSupplemental.

Published November 22, 2023.

biosynthesis gene, *BpMAX1* (*MORE AXILLARY GROWTH 1*). While the role of SL phytohormones in plant architecture, especially their inhibition of branching, is well-established in annual herbaceous plants, it is less well understood in long-living tree species, which have more complex branching patterns (11, 12).

SLs are a structurally diverse class of carotenoid-derived plant hormones; to date, more than 30 different biologically active compounds have been identified (13, 14). They are also exuded by plants into the rhizosphere, where they promote symbiotic interactions with arbuscular mycorrhizal fungi (15, 16) and induce the germination of root parasitic plants of the *Orobanchace* and *Striga* genera (17, 18). Despite their structural variety, all of the elucidated structures of biologically active SLs are characterized by the presence of a butenolide lactone ring (D-ring). In canonical SLs, it is connected by an enol ether bridge to a second moiety that consists of a tricyclic lactone (ABC-ring); in noncanonical SLs, it is connected to other secondary moieties that are not as well conserved (19, 20). The enol ether is unstable and easily cleaved or hydrolyzed, so SLs

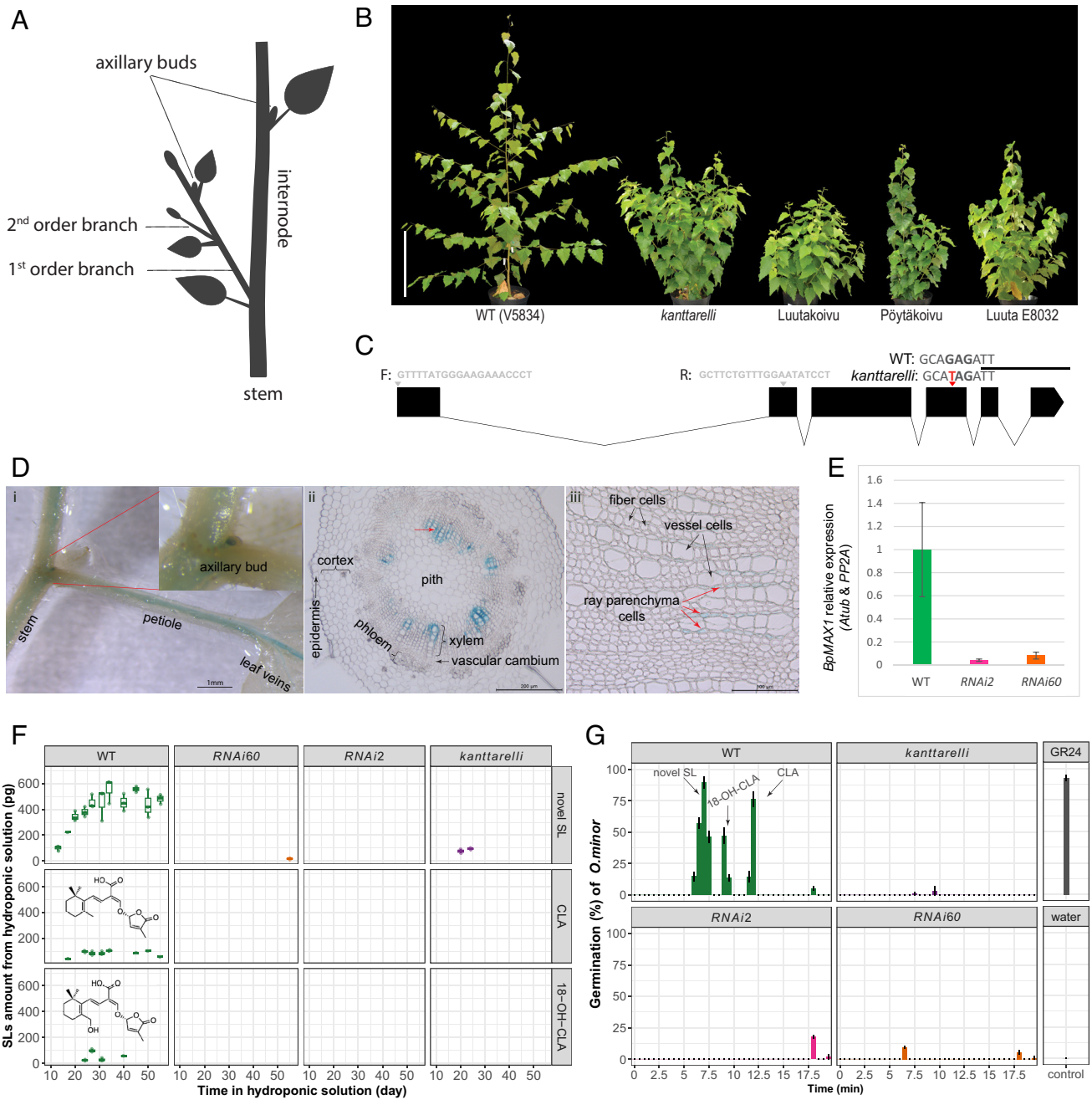

Fig. 1. Identification of the natural *bpmax1* mutant. (*A*) A schematic view of higher-order branches and other major components of a tree crown. (*B*) Phenotypes of 3-mo-old bushy birches grown in greenhouse conditions (Scale bar, 30 cm.) (*C*) Gene structure of *BpMAX1*; F and R are the primer positions designed for the *RNAi* construct; the *kanttarelli* mutation is highlighted in the fourth exon, showing a single nucleotide polymorphism (G -> T) causing an early stop codon (Scale bar, 500 bases.) (*D*) Histochemical GUS staining of *pBpMAX1::GUS* plants. Panel *i*) a representative shoot of *in vitro pBpMAX1::GUS* (Scale bar, 1 mm.) The upper right corner of the image features a magnified view, highlighting the axillary bud. Panel *ii*) a representative stem of in vitro *pBpMAX1::GUS* (Scale bar, 200 μm.) Panel *iii*) internode5 of a branch from a 2-mo-old greenhouse-grown *pBpMAX1::GUS* tree (Scale bar, 100 μm.) Tissues and xylem cell types in the vasculature are marked in the figure. Ray parenchyma cells are highlighted with red arrows. (*E*) qRT-PCR analysis of *BpMAX1* expression, with the reference genes *PP2A* and *Atub*, $n = 3$, error bars show SEM. A *t*-test was performed to compare *BpMAX1* expression. $P = 0.078$ (WT vs. *RNAi2*), $P = 0.087$ (WT vs. *RNAi60*). (*F*) Birch SL quantification throughout 2 mo, $n = 9$. Structures of CLA and 18-OH-CLA are shown in the WT column. (*G*) Germination response of *Orobanche minor* seeds to birch SLs, $n = 3$, error bars show SD. There are three germination peaks from a previously uncharacterized potential SL, 18-OH-CLA, and CLA at t_R 6.9 min, 9.8 min, and 11.9 min, respectively.

exhibit a major common fragment ion at *m/z* 97 in liquid chromatography with tandem mass spectrometry (LC–MS/MS) reflecting the D-ring moiety.

In the SL synthesis pathway, *MAX1*, *MAX3*, and *MAX4* are the three best-characterized SL biosynthesis genes in *Arabidopsis*. Previous studies have suggested that MAX3 and MAX4 are carotenoid dioxygenases, while MAX1 belongs to the cytochrome P450 family (21–23). Other growth regulators that have been implicated in the regulation of branching include auxin and sucrose. Auxin has been proposed to inhibit lateral branching through two parallel (and not mutually exclusive) mechanisms, a canalization-based and a secondary messenger model (24). Sucrose has also been indicated to trigger bud outgrowth and antagonize the effect of auxin and SLs on bud outgrowth (25, 26).

Our study explores the links between tree architectural development and SL content, auxin and sucrose distribution in WT, and SL-deficient birch lines. We combine physiological studies with a modeling approach to form a detailed analysis of the branching pattern in a tree species.

Results

***kanttarelli* Is a Naturally Occurring SL-deficient Birch Mutant.** To understand the genetic basis of tree architecture, we identified four natural bushy variants of *B. pendula* in Finland, namely *kanttarelli*, "Luutakoivu," "Pöytäkoivu," and "Luuta E8032" (Fig. 1*B*), and we studied their branching patterns under greenhouse conditions. During 3 mo of growth, all of the bushy variants were shorter than the designated WT V5834 (a *B. pendula* clone from the Finnish breeding population) in the greenhouse. Meanwhile, all the birches in this experiment formed first-order branches in 3 wk. Luutakoivu had more first-order branches than the WT. In contrast, Pöytäkoivu and Luuta E8032 had fewer first-order branches than the WT. Intriguingly, *kanttarelli* birch (from Kuopio, Finland, 60°90′N, 27°62′E) had a similar number of first-order branches and internodes in its main stem as the WT (*SI Appendix*, Fig. S1) even though the main stem of *kanttarelli* was shorter. By systematically searching in *kanttarelli*, Luutakoivu and Pöytäkoivu for disruptive mutations in candidate genes that share homology with previously identified branching-linked genes in other plant species (7), we identified a loss-of-function mutation due to an early stop codon in the fourth exon of *BpMAX1*, an ortholog of the *Arabidopsis MORE AXILLARY GROWTH 1* (*AtMAX1*) gene (Fig. 1*C* and *SI Appendix*, Fig. S2*A* and Table S2) in the *kanttarelli* variant. In contrast to *kanttarelli*, we did not find disruptive mutations in the SL-related genes in the other bushy variants.

BpMAX1 is the only ortholog of *AtMAX1* in the silver birch genome (*SI Appendix*, Fig. S2*B*); its protein sequence is 74.2% identical with the AtMAX1 protein (*SI Appendix*, Fig. S2*C*). To investigate the conservation of *BpMAX1* and its promotor *pBpMAX1*, a complementation assay was performed in *Arabidopsis*. Both branch number (*SI Appendix*, Fig. S2 *D* and *E*) and plant height (*SI Appendix*, Fig. S2 *F* and *G*) phenotypes were rescued in the *Arabidopsis max1* mutant by the expression of a *pBpMAX1::BpMAX1* construct.

To assess the pattern of *BpMAX1* expression, we generated a promoter-*GUS* reporter construct, *pBpMAX1::GUS*, using 2,215 bp of the genomic sequence upstream of the *BpMAX1* transcription start site. In the shoot, *pBpMAX1::GUS* was expressed in both the vasculature and the axillary buds. In the vasculature, it was observed to be prominently expressed in the ray parenchyma cells (Fig. 1*D*). This result is consistent with published birch RNAseq data (8), where the *BpMAX1* transcript also peaks in the xylem tissue (*SI Appendix*, Fig. S3 *A* and *D*). Furthermore, the other two orthologs of SL biosynthetic genes in birch, *BpMAX3* and *BpMAX4,* are also expressed specifically within the xylem (*SI Appendix*, Fig. S3 *B–D*). Previous studies in *Arabidopsis* have shown that genes involved in SL production and response are expressed in both shoot and root vascular tissues (23, 27–29). This indicates that birch may be able to produce SL and/or its biosynthetic intermediates in the context of xylem tissues.

To test whether the *kanttarelli* phenotype results from the naturally occurring mutation in the *BpMAX1* gene, we used RNA interference (RNAi) to generate transgenic birch lines with downregulated *BpMAX1* expression in the designated WT. Suppression of *BpMAX1* expression was achieved by generating an RNAi construct targeting a 336-bp fragment from the first exon to the beginning of the second exon (Fig. 1*C*). Transcription levels of *BpMAX1* in the representative downregulation lines (*RNAi60* and *RNAi2*) were reduced compared with WT (Fig. 1*E*).

To examine whether SL content was downregulated in the *RNAi60* and *RNAi2* lines, we profiled SL in root exudates of these lines as well as in *kanttarelli*. We observed that *RNAi60*, *RNAi2*, and *kanttarelli* produced very limited SL compared to the WT during 2 mo of growth in hydroponic solutions (Fig. 1*F* and *SI Appendix*, Fig. S4 *A–D*). Two SL compounds, carlactonoic acid (CLA) and 18-hydroxycarlactonoic acid (18-OH-CLA) (*SI Appendix*, Fig. S4*A*), were identified in the birch root exudates by comparing their retention times (t_R) in LC–MS/MS with the corresponding synthetic standards. We then confirmed their identity and function by testing their ability to promote the germination of *O. minor* seeds, a standard bioassay for SL activity (13, 18, 30). The germination assay also identified another active germination stimulant with a t_R of 6.9 min (Fig. 1*G*). The stimulant had major fragment ions at *m/z* 97 (*SI Appendix*, Fig. S4*E*), characteristic of a SL D-ring moiety, indicating that this is a previously uncharacterized SL. The biological assay not only verified the retention times of the birch SLs but also validated reduced SL levels in *RNAi60*, *RNAi2*, and *kanttarelli*, since their root extracts had much lower *O. minor* germination promotion activity (Fig. 1*G*). Collectively, these results indicate that *kanttarelli* is indeed a natural SL mutant and that we successfully generated SL downregulation lines by silencing *BpMAX1.*

SLs Affect Tree Architecture By Regulating Higher-order Branching. To better characterize the bushy phenotypes of the various genetic lines with reduced *BpMAX1* activity, we documented the growth of WT, *RNAi60*, *RNAi2*, and *kanttarelli* under greenhouse conditions for 1 y (Fig. 2*A*). Similarly to previous studies in other species (23, 30–32), the *BpMAX1::RNAi* lines and *kanttarelli* were shorter than the WT (*SI Appendix*, Fig. S5*A*). Unlike herbaceous SL mutants (in *Arabidopsis*, rice, and pea), which had more first-order branches (23, 30–32), the *BpMAX1::RNAi* lines had a very similar number of first-order branches as the WT (Fig. 2*F*). It should be noted that in WT birch seedlings, most of the axillary buds on the main stem usually form primary branches, so there is little opportunity for an increase in first-order branching. However, whereas the WT formed very few second-order branches during the first year, both *RNAi60* and *RNAi2* developed several second-order branches (Fig. 2*G*), indicating that SL deficiency promotes secondary axillary bud growth.

Another characteristic feature of SL deficiency in herbaceous species is reduced branch angle (33, 34). To evaluate this phenotype in birch, we performed a 3D terrestrial laser-scanning (3D-TLS) experiment (35–37) on greenhouse-grown 14-wk-old plants and again after the onset of dormancy in the first winter. The results showed that *BpMAX1::RNAi* lines had smaller branch angles than the WT (*SI Appendix*, Fig. S5 *B* and *C*). The shorter stems, higher branching order, and more erect branches in *BpMAX1::RNAi*

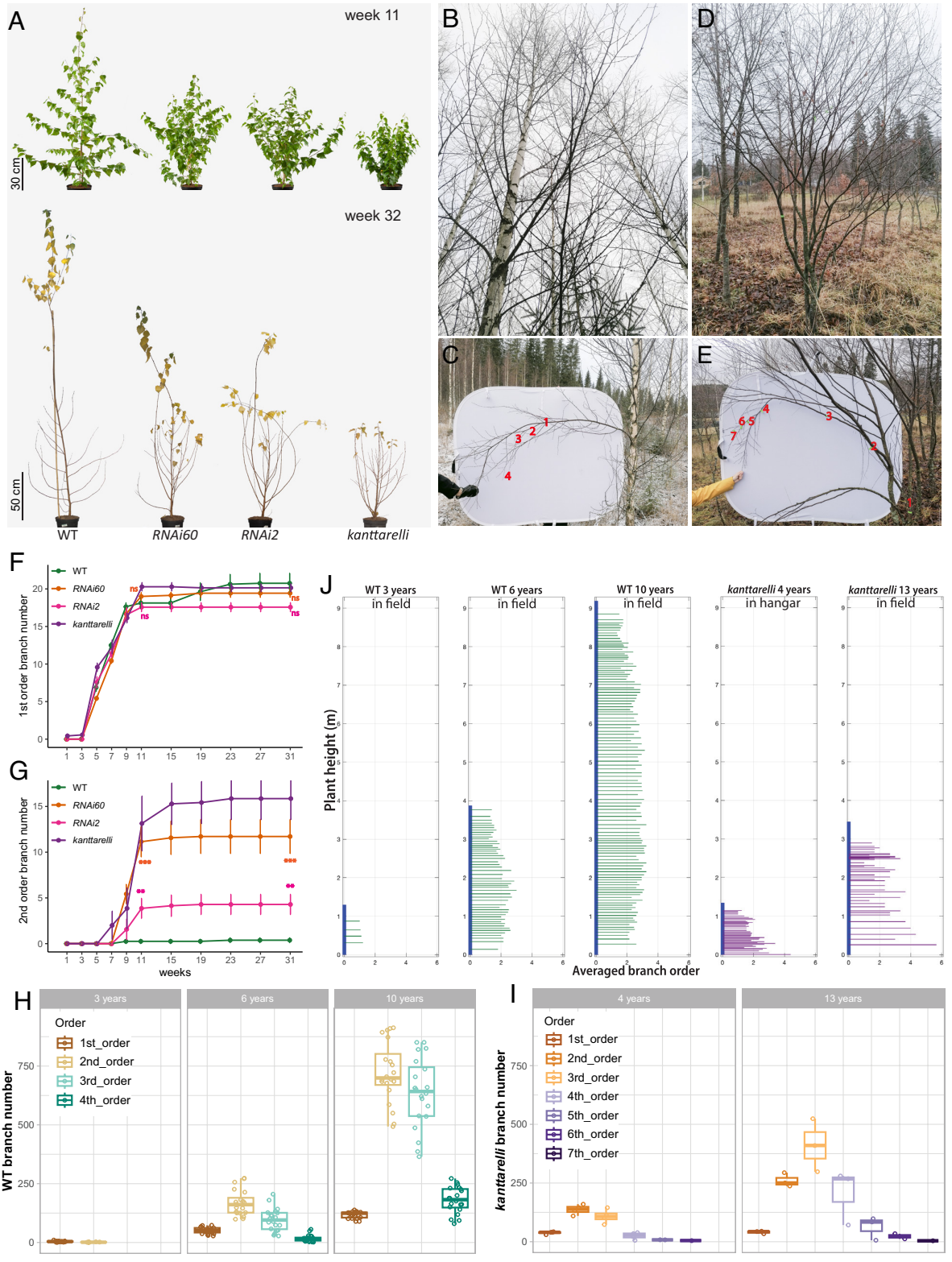

Fig. 2. Increased higher-order branching in *BpMAX1::RNAi* lines and *kanttarelli* vs. WT. (*A*) *Upper*: Phenotypes of WT, *RNAi60*, *RNAi2*, and *kanttarelli* at week 14 in the greenhouse. *Lower*: Phenotypes of WT, *RNAi60*, *RNAi2*, and *kanttarelli* at week 32 in the greenhouse. The WT was held in place by a vertical stick. (*B*) Phenotype of 10-y-old WT-looking bred population of birch trees in the field. (*C*) A close-up view of the highest-order branching of a 10-y-old birch tree from the field. The branch order is indicated with red numbers. (*D*) Phenotype of a 13-y-old *kanttarelli* in the field. (*E*) A close-up view of the highest-order branching of a 13-y-old *kanttarelli*. The branch order is indicated with red numbers. (*F*) Quantification of the number of first-order branches of WT, *RNAi60*, *RNAi2*, and *kanttarelli* throughout 31 wk. The *t*-test was performed on the data from week 11 and week 31; $7 \le n \le 8$; error bars show SEM. (*G*) Quantification of the number of second-order branches of WT, *RNAi60*, *RNAi2*, and *kanttarelli* throughout 31 wk. The t-test was performed on the data from week 11 and week 31; $7 \le n \le 8$; error bars show SEM. (*H*) Quantification of the number of branches per order of a WT-looking bred population of birch trees (abbreviated WT in the figure) in the field, $n = 20$. (*I*) Quantification of the number of branches per order of *kanttarelli*, $3 \le n \le 4$. (*J*) A schematic model of tree architecture: trees vs. bushes. The *x*-axis represents averaged branch orders; the *y*-axis represents plant height. Vertical thick blue lines are stems; the horizontal thin green (WT-looking bred population of birch trees, abbreviated WT in the figure) and purple (*kanttarelli*) lines are the first-order branches carrying higher-order branches. The further the horizontal thin lines reach, the higher order branches they have.

resulted in a rounder and more compact form than the WT (*SI Appendix*, Fig. S5 *D*–*G*). These parameters were analyzed by the NaPPI facility (the National Plant Phenotyping Infrastructure) (38).

To better understand how SL deficiency influences the architecture of birch, we followed the development of tree architecture over time in a WT-looking bred population of birch trees and in the *kanttarelli* mutant. The bred birch population was grown in three stands in Southern Finland (Hollola): a 3-y-old, 6-y-old, and 10-y-old stand. We conducted 3D-TLS scans of these stands. The scanning data revealed that 3-y-old trees of the bred population (avg. height 1.3 m) rarely had any second-order branches, while the 6-y-old (avg. height 3.9 m) and 10-y-old trees (avg. height 9.2 m) had fourth-order branches (Fig. 2 *C* and *H* and *SI Appendix*, Fig. S5*H*).

To understand the role of *BpMAX1* in defining tree architecture, we analyzed the branching pattern in young and old *kanttarelli* trees. We compared 6-y-old trees of the bred population with 4-y-old *kanttarelli* growing in an open-air hangar in Haapastensyrjä's research infrastructure in Loppi, and 10-y-old trees of the bred population with 13-y-old *kanttarelli* growing in the field in Kuopio. The branching pattern of *kanttarelli* contrasted with the trees of the bred population. The scanning data revealed a maximum of sixth-order branches in 4-y-old mutant plants (avg. height 1.4 m) and a maximum of seventh-order branches in 13-y-old mutant plants (avg. height 3.4 m) (Fig. 2 *E* and *I* and *SI Appendix*, Fig. S5*H*), while the WT plants never exceeded fourth-order branching in the period of this study. In conclusion, we observed consistently higher-order branching in the *kanttarelli* mutant than in the bred population in both young and old trees. Additionally, *kanttarelli* exhibited smaller branch angles at young stages than trees in the bred population. In older trees, the branch angles of the two lines were similar (*SI Appendix*, Fig. S5 *I* and *J*). To quantify the higher-order branching phenotype over time, we computed the branch distribution model (Fig. 2*J*). Our model highlights that shorter stems and advanced higher-order branching are two elements that distinguish the architecture of a tree versus a bush.

SL Levels Affect the Auxin Distribution Along the Main Stem. Classical decapitation experiments have shown that the removal of the shoot apex (the auxin source) can activate branching (39–41). To mimic the higher-order branching phenotype in the WT at an earlier stage, we performed a decapitation assay and explored the most efficient way to induce branching in birch. This strategy was chosen due to the complex architecture of birch. The assay included three treatments: i) stem tip removal; ii) first-order branch tip removal from the seven basal branches; iii) a combination of both treatments (*SI Appendix*, Fig. S6*A*). One-month-old WT and *RNAi60* lines underwent all three treatments, and 1 mo after the treatments, we then measured how many second-order branches had grown on first-order branches that had been decapitated. Intact WT did not have second-order branches; some WT that underwent treatments i and ii had second-order branches; all the WT undergoing treatment iii had second-order branches at an early stage. In contrast, *RNAi60* always had second-order branches, with or without the decapitation treatments (*SI Appendix*, Fig. S6 *B* and *C*).

Previous studies have indicated that auxin may act through SLs to facilitate apical dominance and that mutations impairing SL activity significantly increase polar auxin transport (PAT) from the apical to the basal end of excised stem segments (42–45). We therefore analyzed PAT in internodes from the upper half of WT, *RNAi60*, and *kanttarelli* stems. These three lines exhibited similar patterns of PAT, with decreasing PAT from the tip to the middle of the stems (*SI Appendix*, Fig. S7*A*). Quantification of internode3, internode7, and internode11 from WT and *RNAi60* showed no statistical difference between stem cross-sectional area in the two lines (*SI Appendix*, Fig. S7 *B* and *C*).

To further understand the interaction between auxin and SL, we investigated the auxin content in the primary stem. Auxin profiling was conducted in two sets of experiments. In the first set (in 2021), IAA levels were quantified in internode3, internode7, and internode11 from the top to the middle of 2-mo-old trees (Fig. 3*D*). We observed a reduction in IAA concentration from the top to the middle in the WT. By contrast, we observed little, if any, reduction in *RNAi60* and an increase of IAA concentration in the *kanttarelli* mutant (Fig. 3*A*). In the second set (in 2022), the IAA profile was investigated in both intact and decapitated trees to understand how auxin changes after the initiation of second-order branching. Treatment iii [with both stem and branch tips removed (*SI Appendix*, Fig. S6*A*)] was applied to 1-mo-old WT and *RNAi60* trees. One month later, we sampled the decapitated trees and intact controls. Samples were taken from the tip to the base at four internode intervals (Fig. 3*E*). We observed an alteration of the auxin distribution pattern in the WT after decapitation. Decapitated WT plants with higher-order branches showed an increase in IAA concentration from the top to base (Fig. 3*B*), similar to the intact *RNAi60* (in 2022) and *kanttarelli* previously tested in 2021.

Sucrose has been reported to be another major regulator of branching (25, 46). Therefore, we explored the sucrose distribution in trees and whether it was affected by decapitation. We found that sucrose is evenly distributed from the tip to the base in both intact WT and intact *RNAi60* lines. Moreover, decapitation (treatment iii) did not significantly alter the sucrose distribution pattern in stems (Fig. 3*C*).

Based on our findings, we hypothesized that the structural differences between WT and *RNAi60* may suffice to cause differences in the global auxin concentration pattern, since young expanding leaves at active shoot apices are a major source of auxin in shoots. We used computational modeling to test the plausibility of this hypothesis (Fig. 4). We formally described the following assumptions, which we call the long-distance signaling model (LSM): i) Auxin is synthesized at apices; ii) auxin is synthesized at positions on the branch where leaves are located; iii) auxin is transported basipetally; iv) the magnitude of transport is proportional to the auxin flux; and v) auxin decays at a fixed global rate. This basic LSM model conceptually follows previously published formalisms that simulate long-distance auxin-mediated signaling (47). Structurally, the two lines were designed to have the same number of first-order branches (Fig. 2*F*) and internodes (*SI Appendix*, Fig. S5*K*), following the quantitative phenotyping data of 2-mo-old plants under greenhouse conditions. The main differences were that the *RNAi60* model had shorter internodes than the WT and that the *RNAi60* model had second-order branches while the WT had none (Fig. 4 *A* and *B*).

To model this, we ran a set of simulations with varying configurations of auxin dynamics parameter values, covering a range of plausible values. Each simulation was run until the auxin concentration values between simulation steps reached a steady state. Subsequently, we documented all simulation runs that matched the diverging global auxin concentration patterns that we measured in the WT and *RNAi60* under greenhouse conditions. In Fig. 4*C*, we show a slice of the parameter space of our computational model. Specifically, in the WT, we expect auxin concentration to decrease toward the base of the stem (blue color), while in *RNAi60*, the auxin concentration increased along the stem (red color). A wide range of our in silico experiments generated global auxin concentration patterns along the stem that matched the auxin concentration values observed in vivo. We show an example rendering of our dynamic 3D simulation at homeostasis in Fig. 4*A*, where we used identical parameter value settings for both trees

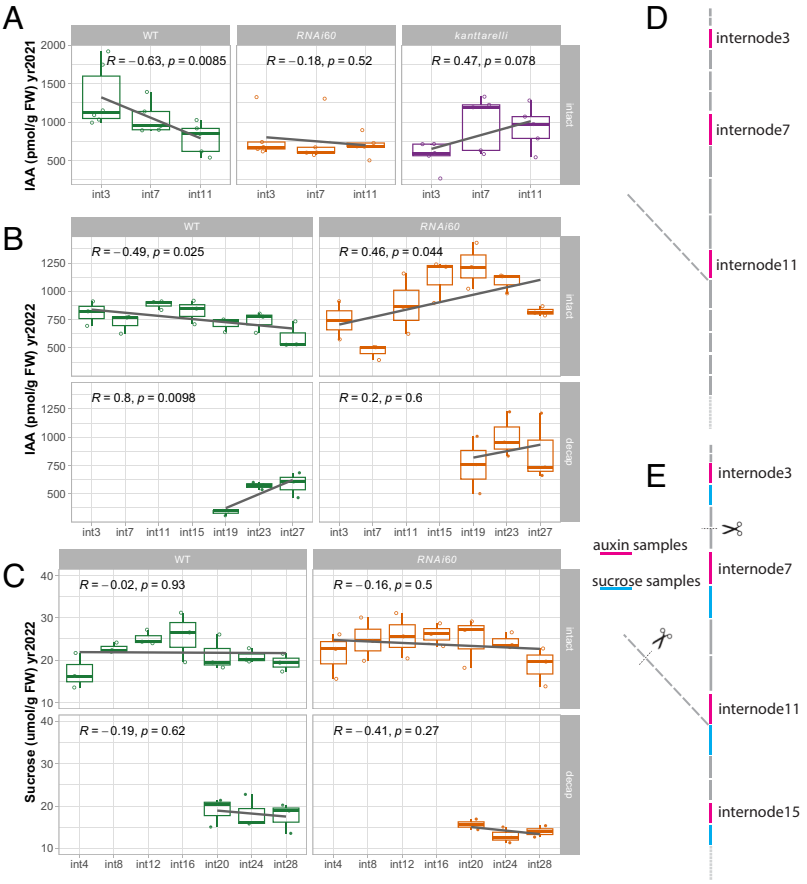

Fig. 3. Auxin distribution along the birch main stem. (*A*) Auxin concentration from the 3rd (uppermost part of the tree) to 11th internode (middle of the tree) of 2-mo-old WT, *RNAi60*, and *kanttarelli* trees in 2021, $n = 5$. (*B*) Auxin concentration from the 3rd (uppermost part of the tree) to 27th internode (base of the stem) of 2-mo-old WT and *RNAi60* in 2022, $n = 3$. Decapitation was performed on 1-mo-old WT and *RNAi60* trees. Sampling took place 1 mo after decapitation to give time for second-order branch development. As a control, 2-mo-old WT and *RNAi60* were sampled together with the decapitated trees. (*C*) Sucrose distribution from the 4th (uppermost part of the tree) to 28th internode (base of the tree) of 2-mo-old WT and *RNAi60* in 2022, $n = 3$. Decapitation and sampling took place at the same time as in Fig. 3*B*. The Pearson correlation coefficient was calculated for the relation between IAA/sucrose levels and the internode position. *r* indicates how far the data points are from the line of the best fit. *p* measures the likelihood of observing a correlation of this strength under the null hypothesis. (*D*) The sample scheme in 2021—auxin samples are in pink and unsampled internodes in gray. (*E*) The sample scheme in 2022—auxin samples are pink, sucrose samples blue, and unsampled internodes gray. More internodes are presented as a lighter gray dashed line at the bottom to represent the complete tree architecture.

($p = 0.7$, $d = 0.155$ in Fig. 4*C*). In this case, the blue color indicates the auxin concentration for a given segment, which declines from the tip to the base in the WT but increases in *RNAi60*. The auxin concentration values (Fig. 4*D*) along the model stems (Fig. 4*A*) were consistent with measurements of the trees under greenhouse conditions (Fig. 3*B*). This implies that under the same auxin synthesis and decay process, global auxin concentrations are more significantly reduced in the WT along the primary axis compared to *RNAi60*, which has shorter internodes and additional auxin sources provided by second-order branches.

The distribution pattern of auxin differs in the WT and *RNAi60*, likely because of architectural differences. We also observed that decapitation altered the distribution of IAA. Therefore, we modeled global auxin concentration patterns in both decapitated WT and *RNAi60* using the same LSM method. The auxin concentration values (Fig. 4*D*) along the decapitated WT stems in the model (Fig. 4*A*) were consistent with the trend of IAA distribution in the experiments conducted under greenhouse conditions (Fig. 3*B*). The auxin concentration gradients in the models mainly result from structural differences, and the greater similarity of the auxin concentration in the decapitation simulations highlights the similar morphology of these plants (*SI Appendix*, Fig. S6*C*). In conclusion, the architectural differences between WT and *RNAi60*—the shorter internodes and increased second-order branching in *RNAi60*—are sufficient to cause different auxin distribution patterns.

Discussion

To address a major question in tree biology: "What separates a tree from a bush?," we took advantage of architectural variation present in birch species. Through a candidate gene approach, we identified a natural mutant, *kanttarelli*, with deficient SL biosynthesis because of a mutation in *BpMAX1*. We found that *pBpMAX1::GUS* was expressed specifically in xylem ray parenchyma cells (Fig. 1*D*), indicating that ray parenchyma cells may contribute to SL synthesis. Previously, grafting experiments had suggested that SL synthetic genes control long-distance and graft-transmissible signals that move upward (21, 48–52). It is a reasonable hypothesis that SL intermediates travel in the xylem. Moreover, orobanchol, a SL compound, was detected in xylem sap in *Arabidopsis* and tomato (53) evidence that SLs are transported through the xylem, at least orobanchol. In this study, we have shown that *BpMAX1* is strongly expressed in the xylem-associated ray parenchyma cells, an essential tissue for the storage and transport of water, nutrients, and nonstructural carbohydrates (NSC) (54). The spatial expression of *BpMAX1* is consistent with the idea of acropetal movement of SLs

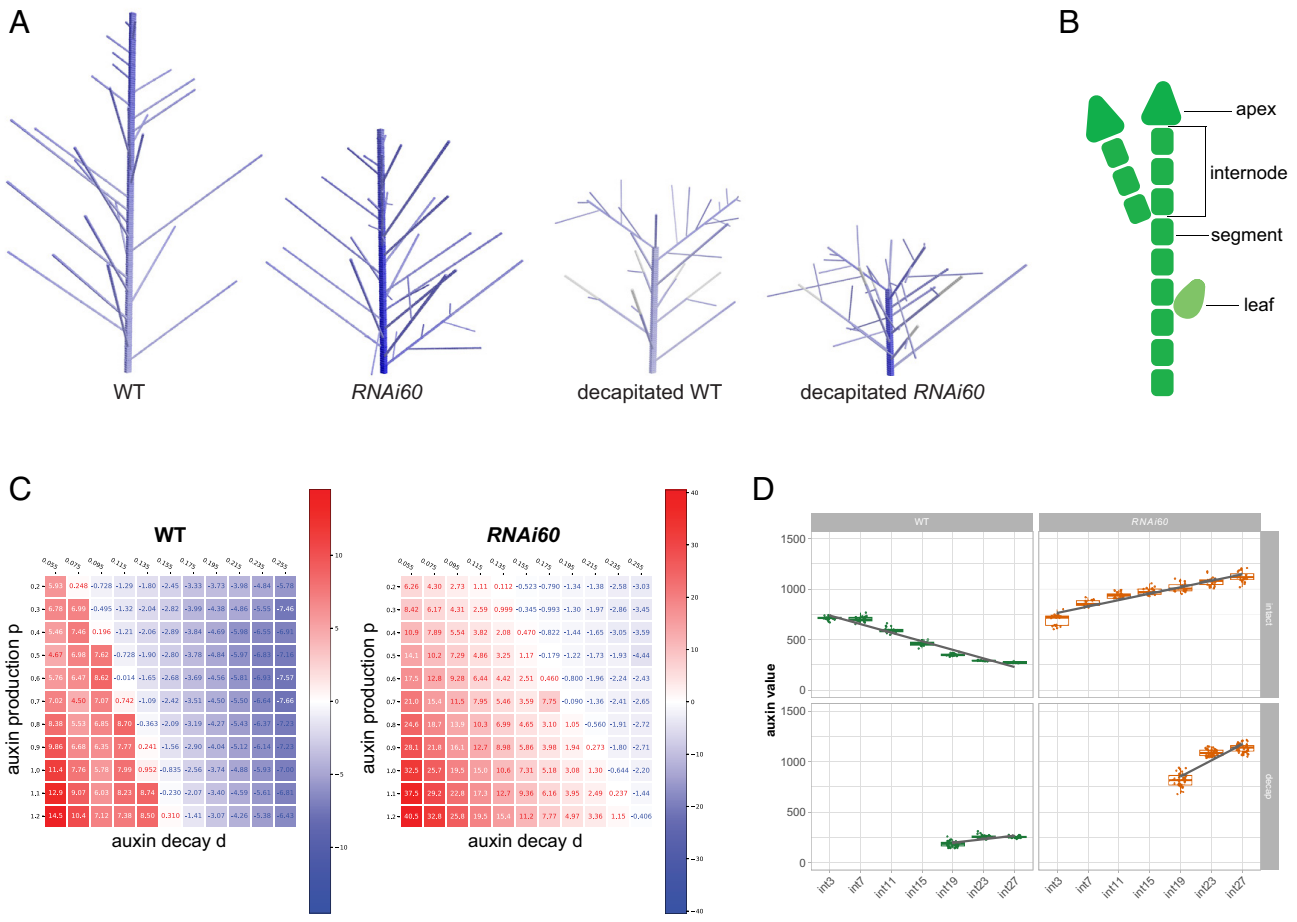

Fig. 4. Computational model simulating auxin transport for WT and *RNAi60*. (*A*) Model structure of intact WT and *RNAi60* trees, and decapitated WT and *RNAi60*. *RNAi60* has shorter internodes than the WT and more second-order branches than WT; decapitation induced second-order branch development in both lines. The schematic models are also examples of 3D simulations of auxin concentration values in the WT and *RNAi60* reached steady state. The blue color denotes the auxin concentration. (*B*) Simulated trees represented as a connected graph of vertices representing branch segments, apices, and/or leaves. Six segments were used to represent an internode in the WT and four segments for an internode in *RNAi60*. (*C*) Each cell in the grid represents an individual simulation run under the specified parameter value settings until homeostasis. Red color denotes a positive and blue color a negative gradient of auxin concentration. (*D*) Stimulated auxin concentration values in model stems. Data are presented also in (*A*).

in plants to regulate shoot branching. Furthermore, highlighting the diversity of naturally occurring SL forms in different plant species, we found that birch most probably contains previously unidentified noncanonical SLs (exhibiting mass fragments of *m/z* 97, *m/z* 139, and *m/z* 157) (*SI Appendix*, Fig. S4*E*), which have not been structurally studied in detail.

Due to the long lifespan of woody species, understanding tree architecture requires long-term observation. In this study, we conducted a detailed phenotyping of young greenhouse-grown SL-deficient birch saplings (Fig. 2 *A*, *F*, and *G* and *SI Appendix*, Fig. S5*A*). Subsequently, we tracked the development of tree architecture over time by 3D laser scanning of field-grown WT and *kanttarelli* trees (Fig. 2 *B*–*E* and *H*–*J* and *SI Appendix*, Fig. S5*H*). Taken together, our data show that the appearance of bushiness in the *kanttarelli* mutant is due to the combined effect of its shorter stature and accelerated higher-order branching under both greenhouse and field conditions.

Previous studies in various species have shown that SL mutants have significantly increased PAT, with 1.5-cm stem segments typically transporting on the order of 20% more auxin than the wild type in six-hour assays (42–45). However, our study revealed similar PAT in the upper half of stems from WT, *RNAi60*, and *kanttarelli*. This could reflect little or no effect of SLs on auxin transport in birch or insufficient sensitivity in the assay. The lack of a discernible difference in auxin transport is not due to gross differences in stem anatomy, since the upper half of the stem appears to have similar anatomy in both WT and *RNAi60* (*SI Appendix*, Fig. S7 *B* and *C*). IAA profiling along the main stem demonstrated that IAA levels and internode position correlate negatively in the WT, consistent with the pattern expected if auxin is synthesized in the apex, transported basipetally, and decays at some rate. The IAA distribution pattern can be altered by decapitation treatment in the WT (Fig. 3 *A* and *B*), with an increase in the number of active apices correlating with increased auxin in more basal internodes, eliminating or even reversing the gradient seen in intact plants. Consistent with this idea, the distribution of auxin in SL-deficient birch is similar to that in decapitated WT trees. Indeed, our computational model suggests that shorter stature and increased second-order branching are sufficient to account for the different auxin distributions in the WT and the SL-deficient lines, with no requirement for differences in auxin synthesis, transport, or decay.

These results are consistent with data from *Arabidopsis*, though there are differences. In birch, the primary shoot is highly branched, with buds released from apical dominance as the primary shoot grows, increasing the distance between it and the axillary buds below it, resulting in a classical acropetal branching habit. In contrast, in *Arabidopsis*, apical dominance during vegetative growth is much

stronger, which is likely in part due to the very short internodes of the rosette, resulting in the close proximity of all axillary buds to the active primary apex. At floral transition, rapid internode elongation, coupled with the suppression of leaf development, correlates with a dramatic reduction in apical dominance, with axillary buds released in a basipetal pattern (47). This branching is therefore conceptually similar to decapitation, and produces an auxin distribution pattern similar to those seen in decapitated birch (Fig. 3*B*).

The effect of SL deficiency in *Arabidopsis* on these auxin distribution patterns is striking. The gradient of accumulation of auxin down the main stem is much steeper in SL mutants than in the WT, with relatively little difference in auxin levels in apical segments, but approaching an order of magnitude more auxin in basal stem segments of SL-deficient mutants compared to the WT (47). This is qualitatively similar to the situation in birch, with a shift toward greater basal auxin accumulation along the stem in both cases (Fig. 3 *A* and *B*). However, in *Arabidopsis*, the magnitude of the shift cannot be explained solely by differences in stem length and active shoot number since these do not differ greatly between SL mutants and WT at the nodes where auxin has been measured, though the differences in auxin levels are large. In *Arabidopsis*, the auxin differences can be explained by changes in auxin transport, which is significantly increased in SL-deficient mutants. Interestingly, no differences in auxin transport were detected between WT and SL-deficient lines in birch. SL has at least two modes of action, and it is possible that in birch, its effects on gene expression are more important than any effects on auxin transport.

In conclusion, our study comparing the WT and genetic lines that have reduced *BpMAX1* function highlights a different auxin distribution between the tree-like and bushy plants. It is possible that such a difference in auxin distribution could further contribute to various morphological adaptions in the two architectural forms. From an economical point of view, architecture strongly affects the value of a tree: A tall, straight primary stem with few, thin primary branches provides the best timber material for sawmill products, whereas fruit production and ornamental purposes benefit from the shorter forms with abundant branches. Consequently, we hope that our interdisciplinary study will facilitate genome-based breeding of SL-activity-optimized tree architecture for both timber and horticultural purposes.

Materials and Methods

Silver birch WT clone V5834 was used for transgenic plant generation. Plants for GUS-staining, qRT-PCR quantification, IAA profiling, NaPPI phenotypical analysis, auxin transport capacity analysis, and histological analysis were 2 mo old under greenhouse conditions. Plants for decapitation were 1-mo-old, while plants for second-order branch quantification and sampling were 2-mo-old, and plants for both assays were grown under greenhouse conditions. Plants for SL profiling were hydroponically. Details for the following are available in *SI Appendix, SI Materials and Methods*: genetic materials and growth conditions, histochemical staining for GUS activity, qRT-PCR, *O. minor* germination assay, SL profiling, laser scanning and scanning data analysis, branching distribution modeling, IAA profiling, sucrose profiling, computational model implementation, phylogenetic analysis, NaPPI phenotyping, decapitation assays, polar auxin transport capacity measurement, and stem area measurement. The primers used in this study are listed in *SI Appendix*, Table S1. The *BpMAX1* gene sequence and *kanttarelli* mutation are given in *SI Appendix*, Table S2. The *pBpMAX1* promotor sequence is given in *SI Appendix*, Table S3.

Data, Materials, and Software Availability. Code and script data have been deposited in ChangBio/kanttarelli (https://zenodo.org/badge/633505761.svg) (55). The modeling algorithms, computer code, and R code are available at https://github.com/ChangBio/kanttarelli.git (56). All other data are included in the manuscript and/or *SI Appendix*.

ACKNOWLEDGMENTS. We thank Katja Kainulainen, Leena Grönholm, Puk Klamer, Clemens Raths, Aruto Nakada, Wafaa Kanash, and Elias Päivinen for the excellent technical assistance. Additionally, we thank Thomas Lilja for finding the scanned commercial stands, Nina Heiska for 3D terrestrial laser-scanning and providing the scanning details, and Marco Pisanu for digital analysis support. The work was funded by the European Research Council (ERC SYMDEV 323052, ERC-CoG CORKtheCAMBIA 819422), Academy of Finland Center of Excellence in Molecular Biology of Primary Producers (AoF CoE 271832) and CoE in Tree Biology (TreeBio AoF CoE 346139; 346141), University of Helsinki award (799992091), Gatsby Foundation (GAT3395/PR3 and GAT3272C), Academy Professor (AoF 345137), Jane and Aatos Erkko Foundation (200003), Bill & Melinda Gates Foundation (OPP1207956), Academy Project Funding (AoF 286404 and 322690, Chinese Government Scholarship (201506600037), European Union's Horizon 2020 project PlantaSYST (SGA-CSA No 664621 and No 739582 under FPA No. 664620), European Regional Development Fund-Project (CZ.02.1.01/0.0/0.0/16_019/0000827), Academy of Finland Postdoctoral Researcher (AoF 326036), Academy Research Fellow (AoF 347130 and 353537), Suomen Luonnonvarain tutkimussäätiö (SLTS 20220013/20230059), Knut and Alice Wallenberg Foundation (KAW 2016.0352 and KAW 2020.0240), and Swedish Governmental Agency for Innovation Systems (VINNOVA 2016-00504).

Author affiliations: [a]Organismal and Evolutionary Biology Research Program, Faculty of Biological and Environmental Sciences, Viikki Plant Science Centre, University of Helsinki, Helsinki 00014, Finland; [b]Institute of Biotechnology, Helsinki Institute of Life Science, University of Helsinki, Helsinki 00014, Finland; [c]Mathematics and Computer Science, Adam Mickiewicz University, Poznań 61-614, Poland; [d]Center for Bioscience Research and Education, Utsunomiya University, Utsunomiya 321-8505, Japan; [e]Laboratory of Growth Regulators, Institute of Experimental Botany of the Czech Academy of Sciences, Faculty of Science of Palacký University, Olomouc CZ-78371, Czech Republic; [f]Max-Planck-Institute of Molecular Plant Physiology, Potsdam-Golm 14476, Germany; [g]Center of Plant Systems Biology and Biotechnology, 4000 Plovdiv, Bulgaria; [h]Mathematics, Tampere University, Tampere 33720, Finland; [i]Key Laboratory of Horticultural Plant Biology of Ministry of Education, College of Horticulture and Forestry Sciences, Huazhong Agricultural University, Wuhan 430070, China; [j]Production Systems, Natural Resources Institute Finland (Luke), Helsinki 00790, Finland; [k]Molecular and Integrative Biosciences Research Program, Faculty of Biological and Environmental Sciences, and Viikki Plant Science Centre, University of Helsinki, Helsinki 00014, Finland; [l]Laboratoire de Reproduction et Développement des Plantes, École Normale Supérieure de Lyon, Institut National de la Recherche Agronomique, Lyon 69342, France; [m]Biosciences Division, Oak Ridge National Laboratory, Oak Ridge, TN 37830; [n]National Plant Phenotyping Infrastructure, Helsinki Institute of Life Science, University of Helsinki, Biocenter Finland, Helsinki 00014, Finland; [o]Department of Forest Genetics and Plant Physiology, Umeå Plant Science Centre, Swedish University of Agricultural Sciences, 90183 Umeå, Sweden; [p]Sainsbury Laboratory, University of Cambridge, Cambridge CB2 1LR, United Kingdom; [q]School of Biological Sciences, Nanyang Technological University, Singapore 637551, Singapore; and [r]Centre of the Region Haná for Biotechnological and Agricultural Research, Faculty of Science, Palacký University and Institute of Experimental Botany of the Academy of Sciences of the Czech Republic, Olomouc 78371, Czech Republic

Author contributions: C.S., Y.H., and K.N. designed research; C.S., A.K., X.X., A.P., Y.Z., P.R., X.S., S.M., M.K.T., J.I., R.H., O.S., J.A.-S., G.E., and M.P.V. performed research; C.S. contributed new reagents/analytic tools; C.S., A.K., P.R., X.S., K.L., S.W., A.P.M., K.H., J.S., A.R.F., O.N., O.L., and W.P. analyzed data; K.L. and O.N. supervision of auxin measurement; S.W. supervision of PAT measurement; A.P.M. interpretation of experiments; K.H. supervision of NaPPI measurement; J.S. supervision of bioinformatics analysis; A.R.F. supervision of sugar measurement and manuscript revision; O.L. interpretation of experiments and manuscript revision; W.P. supervision of auxin dynamics computational model generation, manuscript preparation, and revision; C.S., Y.H., and K.N. study conception and design, analysis and interpretation of experiments, manuscript preparation and revision; and C.S. wrote the paper.

1. R. J. Petit, A. Hampe, Some evolutionary consequences of being a tree. *Annu. Rev. Ecol. Evol. Syst.* **37**, 187–214 (2006).
2. J. W. Leverenz, Photosynthesis and transpiration in large forest-grown Douglas-fir: Interactions with apical control. *Can. J. Bot.* **59**, 2568–2576 (1981).
3. A. A. Suzuki, Shoot growth patterns in saplings of *Cleyera japonica* in relation to light and architectural position. *Tree Physiol.* **23**, 67–71 (2003).
4. L. Maillette, Structural dynamics of silver Birch. I. The fates of buds. *J. Appl. Ecol.* **19**, 203–218 (1982).
5. A. A. Suzuki, M. Suzuki, Why do lower order branches show greater shoot growth than higher order branches? Considering space availability as a factor affecting shoot growth. *Trees* **23**, 69–77 (2009).
6. W. C. Galinat, The phytomer in relation to floral homologies in the American Maydeae. *Bot. Mus. Leafl., Harv. Univ.* **19**, 1–32 (1959).
7. J. Salojarvi *et al.*, Genome sequencing and population genomic analyses provide insights into the adaptive landscape of silver birch. *Nat. Genet.* **49**, 904 (2017).
8. J. Alonso-Serra *et al.*, Tissue-specific study across the stem reveals the chemistry and transcriptome dynamics of birch bark. *New Phytol.* **222**, 1816–1831 (2019).

9. K. A. Longman, P. F. Wareing, Early induction of flowering in birch seedlings. *Nature* **184**, 2037–2038 (1959).
10. K. Keinonen-Mettälä, A. Pappinen, K. von Weissenberg, Comparisons of the efficiency of some promoters in silver birch (*Betula pendula*). *Plant Cell Rep.* **17**, 356–361 (1998).
11. S. P. Ward, J. Salmon, S. J. Hanley, A. Karp, O. Leyser, Using Arabidopsis to study shoot branching in biomass willow. *Plant Physiol.* **162**, 800–811 (2013).
12. J. Salmon, S. P. Ward, S. J. Hanley, O. Leyser, A. Karp, Functional screening of willow alleles in Arabidopsis combined with QTL mapping in willow (Salix) identifies SxMAX4 as a coppicing response gene. *Plant Biotechnol. J.* **12**, 480–491 (2014).
13. X. Xie, Structural diversity of strigolactones and their distribution in the plant kingdom. *J. Pestic. Sci.* **41**, 175–180 (2016).
14. K. Yoneyama *et al.*, Which are the major players, canonical or non-canonical strigolactones? *J. Exp. Bot.* **69**, 2231–2239 (2018).
15. K. Yoneyama, T. Kisugi, X. Xie, K. Yoneyama, "Chemistry of strigolactones: Why and how do plants produce so many strigolactones?" in *Molecular Microbial Ecology of the Rhizosphere* (Wiley, 2013), pp. 373–379, https://doi.org/10.1002/9781118297674.ch34.
16. K. Akiyama, K. Matsuzaki, H. Hayashi, Plant sesquiterpenes induce hyphal branching in arbuscular mycorrhizal fungi. *Nature* **435**, 824–827 (2005).
17. K. Akiyama, H. Hayashi, Strigolactones: Chemical signals for fungal symbionts and parasitic weeds in plant roots. *Ann. Bot.* **97**, 925–931 (2006).
18. R. Matusova *et al.*, The strigolactone germination stimulants of the plant-parasitic *Striga* and *Orobanche* spp. are derived from the carotenoid pathway. *Plant Physiol.* **139**, 920–934 (2005).
19. S. Al-Babili, H. J. Bouwmeester, Strigolactones, a novel carotenoid-derived plant hormone. *Annu. Rev. Plant Biol.* **66**, 161–186 (2015).
20. K.-P. Jia, L. Baz, S. Al-Babili, From carotenoids to strigolactones. *J. Exp. Bot.* **69**, 2189–2204 (2017).
21. K. Sorefan *et al.*, MAX4 and RMS1 are orthologous dioxygenase-like genes that regulate shoot branching in Arabidopsis and pea. *Genes. Dev.* **17**, 1469–1474 (2003).
22. J. Booker *et al.*, MAX3/CCD7 is a carotenoid cleavage dioxygenase required for the synthesis of a novel plant signaling molecule. *Curr. Biol.* **14**, 1232–1238 (2004).
23. J. Booker *et al.*, MAX1 encodes a cytochrome P450 family member that acts downstream of MAX3/4 to produce a carotenoid-derived branch-inhibiting hormone. *Dev. Cell* **8**, 443–449 (2005).
24. M. A. Domagalska, O. Leyser, Signal integration in the control of shoot branching. *Nat. Rev. Mol. Cell Biol.* **12**, 211–221 (2011).
25. M. G. Mason, J. J. Ross, B. A. Babst, B. N. Wienclaw, C. A. Beveridge, Sugar demand, not auxin, is the initial regulator of apical dominance. *Proc. Natl. Acad. Sci. U.S.A.* **111**, 6092–6097 (2014).
26. J. Bertheloot *et al.*, Sugar availability suppresses the auxin-induced strigolactone pathway to promote bud outgrowth. *New Phytol.* **225**, 866–879 (2020).
27. P. Stirnberg, I. J. Furner, H. M. Ottoline Leyser, MAX2 participates in an SCF complex which acts locally at the node to suppress shoot branching. *Plant J.* **50**, 80–94 (2007).
28. H. Shen, P. Luong, E. Huq, The F-Box protein MAX2 functions as a positive regulator of photomorphogenesis in Arabidopsis. *Plant Physiol.* **145**, 1471–1483 (2007).
29. P. B. Brewer *et al.*, LATERAL BRANCHING OXIDOREDUCTASE acts in the final stages of strigolactone biosynthesis in Arabidopsis. *Proc. Natl. Acad. Sci. U.S.A.* **113**, 6301–6306 (2016).
30. V. Gomez-Roldan *et al.*, Strigolactone inhibition of shoot branching. *Nature* **455**, 189–U122 (2008).
31. P. Stirnberg, K. van de Sande, H. M. O. Leyser, MAX1 and MAX2 control shoot lateral branching in Arabidopsis. *Development* **129**, 1131–1141 (2002).
32. M. Umehara *et al.*, Inhibition of shoot branching by new terpenoid plant hormones. *Nature* **455**, 195–200 (2008).
33. T. Bennett *et al.*, Strigolactone regulates shoot development through a core signalling pathway. *Biol. Open* **5**, 1806–1820 (2016).
34. D. Sang *et al.*, Strigolactones regulate rice tiller angle by attenuating shoot gravitropism through inhibiting auxin biosynthesis. *Proc. Natl. Acad. Sci. U.S.A.* **111**, 11199–11204 (2014).
35. K. Calders *et al.*, Terrestrial laser scanning in forest ecology: Expanding the horizon. *Remote Sens. Environ.* **251**, 112102 (2020).
36. P. Raumonen, B. Brede, A. Lau, H. Bartholomeus, "A shortest path based tree isolation method for UAV LiDAR data" in *2021 IEEE International Geoscience and Remote Sensing Symposium (IGARSS)* (2021), pp. 724–727.
37. P. Raumonen *et al.*, Fast automatic precision tree models from terrestrial laser scanner data. *Remote Sens.* **5**, 491–520 (2013).
38. NaPPI (National Plant Phenotyping Infrastructure), https://www.helsinki.fi/en/infrastructures/national-plant-phenotyping. Accessed 3 February 2023.
39. R. Snow, Experiments on growth inhibition. Part II–New phenomena of inhibition. *Proc. R. Soc. Lond. Ser. B, Biol. Sci.* **108**, 305–316 (1931).
40. D. A. Morris, Transport of exogenous auxin in 2-branched dwarf pea-seedlings (*Pisum sativum* L.)–Some implications for polarity and apical dominance. *Planta* **136**, 91–96 (1977).
41. K. V. Thimann, F. Skoog, Studies on the growth hormone of plants: III. The inhibiting action of the growth substance on bud development. *Proc. Natl. Acad. Sci. U.S.A.* **19**, 714–716 (1933).
42. T. Bennett *et al.*, The Arabidopsis MAX pathway controls shoot branching by regulating auxin transport. *Curr. Biol.* **16**, 553–563 (2006).
43. M. Muhr, N. Prufer, M. Paulat, T. Teichmann, Knockdown of strigolactone biosynthesis genes in Populus affects BRANCHED1 expression and shoot architecture. *New Phytol.* **212**, 613–626 (2016).
44. P. B. Brewer, E. A. Dun, B. J. Ferguson, C. Rameau, C. A. Beveridge, Strigolactone acts downstream of auxin to regulate bud outgrowth in pea and Arabidopsis. *Plant Physiol.* **150**, 482–493 (2009).
45. N. Shinohara, C. Taylor, O. Leyser, Strigolactone can promote or inhibit shoot branching by triggering rapid depletion of the auxin efflux protein PIN1 from the plasma membrane. *PLoS Biol.* **11**, e1001474 (2013).
46. F. Fichtner *et al.*, Regulation of shoot branching in Arabidopsis by trehalose 6-phosphate. *New Phytol.* **229**, 2135–2151 (2021).
47. P. Prusinkiewicz *et al.*, Control of bud activation by an auxin transport switch. *Proc. Natl. Acad. Sci. U.S.A.* **106**, 17431–17436 (2009).
48. C. G. N. Turnbull, J. P. Booker, H. M. O. Leyser, Micrografting techniques for testing long-distance signalling in Arabidopsis. *Plant J.* **32**, 255–262 (2002).
49. C. A. Beveridge, J. J. Ross, I. C. Murfet, Branching mutant rms-2 in *Pisum sativum* (Grafting studies and endogenous indole-3-acetic acid levels). *Plant Physiol.* **104**, 953–959 (1994).
50. E. Foo, C. G. N. Turnbull, C. A. Beveridge, Long-distance signaling and the control of branching in therms1 mutant of pea. *Plant Physiol.* **126**, 203–209 (2001).
51. S. E. Morris, C. G. N. Turnbull, I. C. Murfet, C. A. Beveridge, Mutational analysis of branching in pea. Evidence ThatRms1 and Rms5 regulate the same novel signal. *Plant Physiol.* **126**, 1205–1213 (2001).
52. C. Napoli, Highly branched phenotype of the Petunia dad1-1 mutant is reversed by grafting. *Plant Physiol.* **111**, 27–37 (1996).
53. W. Kohlen *et al.*, Strigolactones are transported through the xylem and play a key role in shoot architectural response to phosphate deficiency in nonarbuscular mycorrhizal host Arabidopsis. *Plant Physiol.* **155**, 974–987 (2011).
54. G. von Arx, A. Arzac, J. M. Olano, P. Fonti, Assessing conifer ray parenchyma for ecological studies: Pitfalls and guidelines. *Front. Plant Sci.* **6**, 1016 (2015).
55. C. Su, Zenodo badge. Zenodo. https://zenodo.org/badge/633505761.svg. Deposited 26 July 2023.
56. C. Su, A. Kokosza, ChangBio/kanttarelli. Github. https://github.com/ChangBio/kanttarelli.git. Deposited 26 July 2023.